Computers & Geosciences 134 (2020) 104347

Contents lists available at ScienceDirect

Computers and Geosciences

journal homepage: www.elsevier.com/locate/cageo

MagB_inv: A high performance Matlab program for estimating the magnetic basement relief by inverting magnetic anomalies

Luan Thanh Pham [a,*], Erdinc Oksum [b], David Gómez-Ortiz [c], Thanh Duc Do [a]

[a] Faculty of Physics, VNU University of Science, Vietnam National University, Hanoi, Viet Nam
[b] Süleyman Demirel University, Engineering Faculty, Department of Geophyisical Engineering, 32260, Isparta, Turkey
[c] Department of Biology and Geology, Physics and Inorganic Chemistry, ESCET, Universidad Rey Juan Carlos, Móstoles, Madrid, Spain

ARTICLE INFO

Keywords:
Magnetic inversion
Magnetic basement
Fast fourier transform
Matlab

ABSTRACT

This paper presents a MATLAB based program, including an easy-to-use graphical interface, developed to estimate 3D geometry of magnetic basement interfaces from respective gridded magnetic anomalies by a rapid iterative procedure. The developed code uses an algorithm based on a relationship between the Fourier transforms of the magnetic data and the interface topography. Given the average depth to the magnetic interface and parameters related to the magnetization, the iterative procedure built up in the frequency domain results with accurate depth estimates in a very short computing time. The program is capable of handling large data sets. The convergence in the iterative process is improved by incorporating a high-cut filtering. The iterations stop when either the RMS error between two successive approximations at any step of the iteration has increased relative to the previous step or when the RMS is below a predefined threshold value, or after a specified maximum iterations number. Settings and updating of the input parameters as well as displaying and exporting the interpretation outputs can easily be managed with the interactive control skills supported by the graphical user interface (GUI) of the MagB_inv code. Applicability and efficacy of the algorithm are illustrated on synthetic data from three 3D interface models, the respective inverted depths match the actual depths even in the presence of noise. As a practical example, the algorithm was also applied to observed anomalies of the total magnetic field from NW-Germany. The calculated magnetic basement interface from the real data application is in good agreement with the previously published configurations of the basement of this study area.

1. Introduction

Geometry determination of a three dimensional magnetic interface is one of the major goals of magnetic interpretation. A possible application of such determination could be magnetic crystalline basement topography mapping that is important for hydrocarbon as well as mineral exploration (Martelet et al., 2013; Salem et al., 2014; Abdullahi et al., 2019). There are many geophysical techniques used to solve this problem. A popular approach, known as the statistical spectral method was introduced by Spector and Grant (1970) and used by Hahn et al. (1976), Connard et al. (1983), Blakely (1988), Brimich et al. (2011) and Chen et al. (2016). Maus (1999) and Maus et al. (1999) further expanded the spectral method as robust method for estimating basement relief. The exponential approach by Aydin and Oksum (2010) based on the analytical solution of the exponential equations obtained from the Fourier transformation of the magnetic data is another technique for determining the depth to the magnetic basement from gridded map. However, this gives only a single basement depth which corresponds to the statistical mean of the basement relief of the data region (Aydın and Oksum, 2012; Pham et al., 2019). Werner (1953) introduced an automated depth-estimation technique, called Werner deconvolution. Hansen and Simmonds (1993) extended this technique to multiple 2D sources, and Hansen (2005) later extended to 3D multiple sources. Another automated technique is the Euler deconvolution that was first developed by Thompson (1982) for two-dimensional profile data, and extended by Reid et al. (1990) for gridded data. Aside from the statistical spectral methods, the Werner and Euler deconvolution techniques are also widely used methods to map basement structure (eg. Hartman et al., 1971; Kilty, 1983; Nabighian and Hansen, 2001; Vo, 2003; Al-Garni, 2010; Martelet et al., 2013; Curto et al., 2015; Al-Badani and Al-Wathaf., 2017; among others). Another group of techniques apply Parker's (1972) forward formula to invert magnetic data for the basement

* Corresponding author.
E-mail address: luanpt@hus.edu.vn (L.T. Pham).

https://doi.org/10.1016/j.cageo.2019.104347
Received 23 May 2019; Received in revised form 1 November 2019; Accepted 2 November 2019
Available online 6 November 2019

topography (i.e., Pilkington and Crossley, 1986; Pustisek, 1990; Jiang et al., 2008; Pilkington, 2006; Caratori Tontini et al., 2008; and Zhang et al., 2016). These techniques speed the computation of magnetic anomalies caused by sources with complex topography. Parker's forward formula relates the sum of the Fourier transforms of the interface topography to the Fourier transform of the potential data. Computer programs in MATLAB and FORTRAN languages based on the Parker's formula were published by Gomez–Ortiz and Agarwal (2005) and Shin et al. (2006) to establish from observed gravity anomalies the subsurface structure. Some graphical interactive software programs were also developed by Mendel et al. (2005), Caratori Tontini (2012) and Schettino (2012) to perform forward modeling of magnetic anomalies. The present study deals with inverting magnetic anomalies by means of an iterative process to estimate the 3D magnetic basement topography. The algorithm works in frequency domain, it is developed in MATLAB and includes a user-friendly graphical interface (GUI) to allow the user to manage the required procedures. The program is capable of handling large magnetic data sets and performs fast and accurate computations, so it constitutes a helpful tool for geophysical exploration and deep crustal geophysical.

2. Theory

The 3D Fourier domain expression of the magnetic anomaly due to an uneven, uniform magnetization layer h by Parker (1972) has been used by several authors (Pustisek, 1990; Xia et al., 1991; Blakely, 1995; Jiang et al., 2008):

$$F[\Delta T] = 2\pi M C_m \Theta_m \Theta_f e^{(-|k|z_0)} \sum_{n=1}^{\infty} \frac{(-|k|)^n}{n!} F[h^n] \quad (1)$$

where F[] denotes Fourier transformation of the variable within brackets, ΔT is the total magnetic field, M the magnetization contrast, C_m is the magnetic permeability and equals 10^{-7} H/m in SI system, $k = \sqrt{k_x^2 + k_y^2}$ where k_x and k_y are the wavenumbers along the plane direction, z_0 is the average interface depth, and Θ_m, Θ_f are given by

$$\Theta_m = \hat{m}_z + i\frac{\hat{m}_x k_x + \hat{m}_y k_y}{|k|}$$

$$\Theta_f = \hat{f}_z + i\frac{\hat{f}_x k_x + \hat{f}_y k_y}{|k|}$$

where $\hat{m} = (\hat{m}_x, \hat{m}_y, \hat{m}_z)$ and $\hat{f} = (\hat{f}_x, \hat{f}_y, \hat{f}_z)$ are the magnetization and the ambient field directions, respectively (i.e., Blakely, 1995).

By rearranging Eq. (1), the depth to the undulating interface can be computed from the magnetic anomaly data by means of an iterative inversion procedure given by

$$F[h] = \lim_{t\to\infty} F[h] = -\frac{F[\Delta T]}{2\pi M C_m \Theta_m \Theta_f |k| e^{(-|k|z_0)}} - \sum_{n=2}^{t} \frac{(-|k|)^{n-1}}{n!} F[h^n] \quad (2)$$

where t stands for the iteration step.

This expression can be solved iteratively to find the topography interface h. Iterations begin by making an initial guess value of h, for example, h = 0. This initial guess value is used to evaluate the right-hand side of Eq. (2). An updated estimation of the interface topography can then be obtained by taking the inverse Fourier transform of this quantity. This value then is used again in Eq. (2) to refine topography interface. The difference between two successive approximations of h can be quantified by a root mean square (RMS) error defined by

$$RMS = \sqrt{\frac{\sum_{i=1}^{M}\sum_{j=1}^{N}\left(h_{i,j}^{t+1} - h_{i,j}^{t}\right)^2}{M \times N}} \quad (3)$$

where M and N are the number of grid nodes along the y-axis (north) and x-axis (east) respectively.

The updating process of depth estimates is continued until a specified number of iterations has been completed or the RMS error of two sequential iterations in Eq. (2) satisfy a presumed accuracy or stopped the instant RMS error magnitude exceeds its previous value.

Following Oldenburg (1974), we improved the inversion procedure also by incorporating a high-cut filter to ensure the convergence of series in the above equation and to avoid its instability at high frequencies. This filter is defined by:

$$B(k) = \left\{ \begin{array}{c} 1 \\ \frac{1}{2}\left[1 + \cos\left(\frac{k - 2\pi WH}{2(SH - WH)}\right)\right] \\ 0 \end{array} \right\}, \quad WH \le \begin{array}{l} |k/2\pi| < WH \\ |k/2\pi| \le SH \\ |k/2\pi| > SH \end{array} \quad (4)$$

where WH and SH are the roll-off frequency parameters of the filter. The filter fully passes frequencies lower than WH, partly passes frequencies between WH and SH, and cuts off frequencies higher than SH. The frequency can be expressed as $1/\lambda$, λ being the wavelength in unit of distance. The proper choose of SH/WH can be derived by analyzing the data power spectrum content. A plot of the logarithm power spectrum versus wavenumber usually shows several straight-line segments that decrease in slope with increasing wavenumber. Generally, low radial wavenumbers mainly relate to deep sources, and intermediate radial wavenumbers mostly correspond to shallow ones, while high radial wavenumbers are dominated by noise (Spector and Grant, 1970). Hereby, to assure the series convergence during the iterative procedure, the SH and WH frequencies should correspond to the frequency limit of the linear segment associated with the mean depth.

Use of low-pass filter leads to a loss of high frequency information (Oldenburg, 1974; Pustisek, 1990; Pham et al., 2018), so the high frequency content of magnetic anomalies recalculated from the inverted basement interface do not necessarily match with that of the original anomalies. The inversion method is limited when the source of the magnetic anomalies corresponds to different bodies of narrow extension and located at different shallow depths. The reason is that such bodies distribution generates magnetic anomalies of high amplitude and high frequency. Taking into account that all methods based on the frequency domain technique require the use of a low pass filter to obtain convergence of the iterative process, such a filter can remove part of the high frequency content and reduce the anomaly amplitude of the signal. Under these circumstances, the information retained by the filter would generate an inverted model can differ from the actual geometry.

3. Overview of the MagB_inv GUI

At the beginning, the MagB_inv program pops up a simple graphical interface covering the left half of the screen. The configuration of this main GUI window is illustrated in Fig. 1a. Here the left upper part of the window allows the user to track the mesh information of loaded data, as well as the respective file root. Below this window, an editable table enables the settings for the initial parameters, the filter parameters and the criterion for the termination of the iterative procedure. The remaining part of the window comprises the display area for the input map. Loading the magnetic data set is enabled by the interactive "Import Data" menu located at the topmost left of the window. The program allows the user loading either a grid file compatible with Golden Software Surfer formats (*.grd [Surfer 7 Binary grid/Surfer 6 text grid] or a three columns ascii-file containing gridded Easting/Northing/Field columns (*.dat, *.txt, *.csv). The grid interval of the input data is required to be equal along the east and north directions. The code does not support a blanked grid input.

After successful data loading, information about the active input grid is listed in the uppermost grid info box and a map view of the input is displayed (Fig. 1b). Then the required input parameters related to the

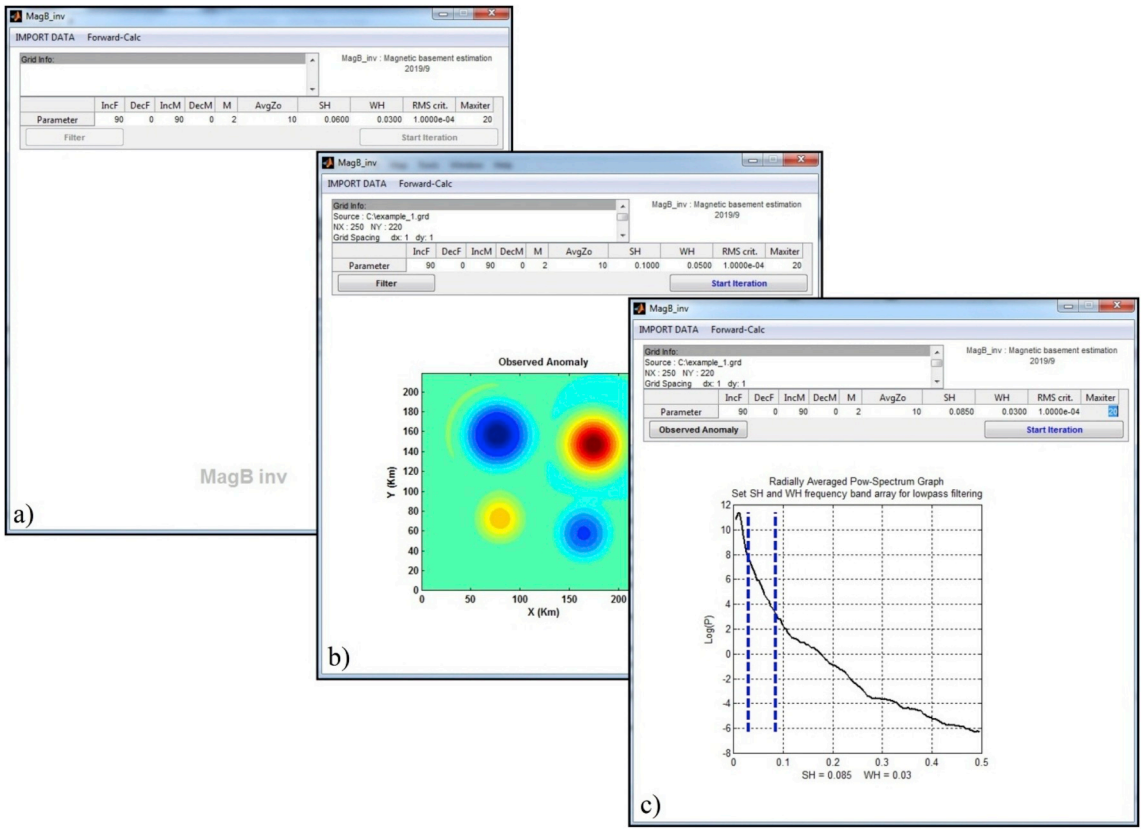

Fig. 1. Screen shot views of MagB_inv GUI, a) the main control window after the first run, b) screen after successful loading of the data and the setting of the initial parameters, c) the window for interactively setting of the low-pass filter parameters prior to start the iteration procedure.

ambient field and magnetization, the average depth of magnetic interface and the roll-off frequency parameters of filtering need to be entered in their related cells of the table component. The units of the magnetic anomalies are nT, magnetization vector directions in degree, magnetization contrast in A/m and distances are in km. The behavior of the termination of the iteration procedure can be set by editing the criterion cell to zero for the divergence-mode or to a non-zero value (default 10^{-4}) for the convergence-mode. In the divergence-mode, the iterative procedure terminates when the RMS error magnitude exceeds its previous value, whereas in the convergence-mode, the iteration stops when the RMS error is below the pre-assigned value. In all cases, however, the iterative procedure stops when the user-defined maximum number of iterations has been attained. The "Filter" menu item enables the user configuring interactively SH and WH frequencies on the radially averaged power spectrum plot of the data (Fig. 1b and c).

After validating range of the inputs, the code calculates the first approximations of the basement depths using the inverse Fourier transform of Eq. (2) evaluated with the initial depths. Then it iterates again Eq. (2) by updating the depth to refine the depth surface. This is iteratively continued until the termination criteria is met. Finally, the code appends the inverted basement depth surface and the respective magnetic response, the difference between the observed and calculated magnetic anomalies, and the RMS errors after each iteration to a temporary *.mat file indexed to the observed input grid. Eventually, the code pops up a new control window next to the main GUI that allows the user to visualize any of the output maps/graphics which can be done as interactively with simple mouse controls (Fig. 2). By preference, any section of the maps can also be illustrated together with profile views. Color on maps and 3D view can be adjusted by tools provided by this control window. All of complete inputs/outputs can be exported either to a user defined file or to a *.mat file comprising the complete inputs/outputs. Maps can be exported to separated *.grd files or in *.dat format in case of the RMS vector and of any extracted profile. Exported *.mat files from MagB_inv code can be reloaded by the "Import Data" main GUI program menu. Thus, saving the data in this way enables one to re-view all the inputs, settings and the interpretation results at any time. Additionally, all the input/output maps and graphics illustrated at the GUI windows can be exported as portable network graphic (*.png) images with a 500 dpi resolution. Additionally to the inversion scheme, the code also includes an in-built GUI window enabled by the "Forward-Calc" menu item to make forward calculation of anomalies of models from given depth grid.

4. Synthetic data application

The program was tested on three synthetic models whose magnetic anomalies were obtained from a same 3D interface model. The intensity of magnetization contrast across the interface is 2.0 A/m. The 3D and the plan view of the model with a mean depth of 10 km is shown in Fig. 3. The first example considers a vertical magnetization model; the second considers a magnetic inclination of 40° and a magnetic declination of −3°; while random noise with amplitude equal to 10% of the anomaly amplitude was added to the third model. The theoretical magnetic anomaly is calculated on a 220× 250 grid with spacing of 1 km along the x and y directions.

The theoretical magnetic anomalies produced by the first simulated model (Fig. 4a) were computed by means of Eq. (1). The data was inverted using the MagB_inv program. The roll-off frequency parameters of the low-pass filter were set to SH = 0.085 and WH = 0.03. The algorithm performed eighteen iterations. It stopped when the RMS error between two successive approximations dropped below a pre-assigned error of 10^{-4} km. The first RMS error value between two successive topography approximations is 0.0107 km and reaches 9.6404×10^{-5} km at the end of 18th iteration (Fig. 4f). The obtained interface is shown

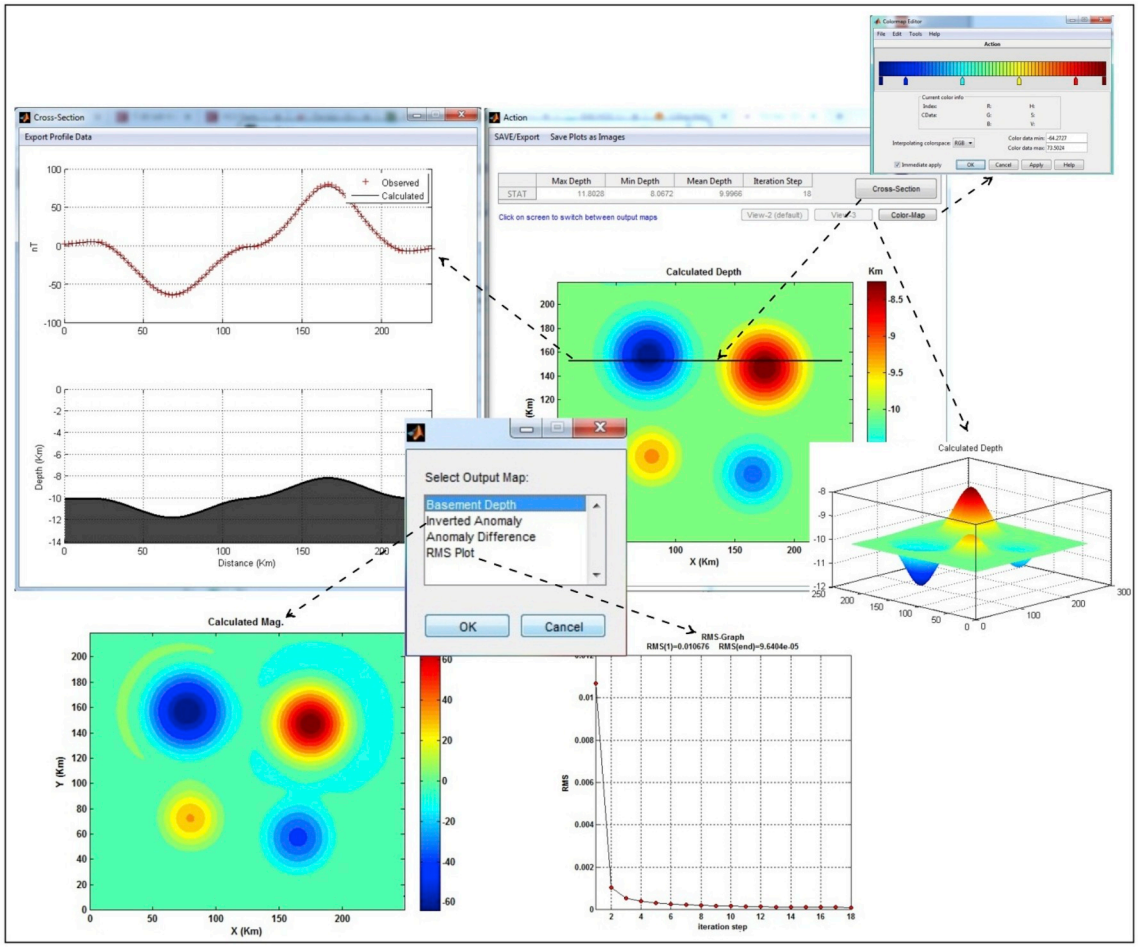

Fig. 2. Screen shot view of the output control panel and some presentative plots after a complete inversion.

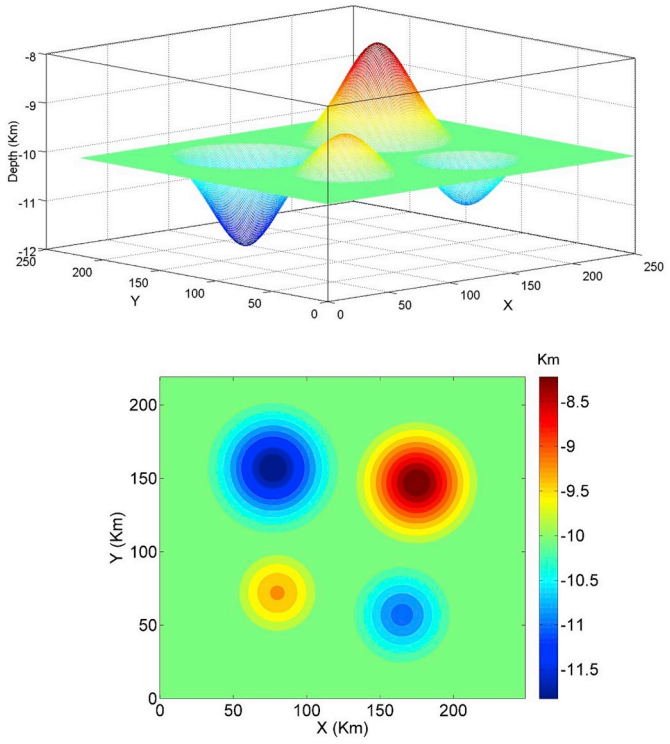

Fig. 3. 3D and plan view of the model interface used to produce synthetic data.

in Fig. 4b. By comparing Figs. 3 and 4b, it is observed that the obtained interface compares reasonably well with the model depth. Fig. 4d shows the difference between the original and the inversion interface of Fig. 4b. The RMS error between them is only 0.0144 km. Accordingly, the magnetic anomaly obtained from the inversion interface compares well with the theoretical magnetic anomaly, as indicated by comparison of Fig. 4a and c. The difference between the actual and calculated magnetic anomalies is shown in Fig. 4e. The inversion of 220×250 observation point mesh in a personal computer with Core(TM) i3 at 2.4 GHz CPU took only 3.3 s, which is a very short time for this kind of calculation.

The MagB_inv program was also applied to this 3D interface model in the case of non-vertical magnetization. The computed magnetic field of the model with an assumed magnetic inclination of 40° and a magnetic declination of −3° is shown in Fig. 5a. The frequency parameters of the low-pass filter have also been chosen as SH = 0.085 and WH = 0.03. After inverting this data, the RMS error between two successive topography approximations has reduced from 0.0107 km to 9.8783×10^{-5} km at the end of 19th iteration (Fig. 5f). Fig. 5b displays the geometry of the inverted magnetic interface. It can be seen from Figs. 3 and 5b that the inversion results are consistent with the theoretical depths. The differences between the inversion results and theoretical models are shown in Fig. 5d, which are insignificantly small with a RMS error between them of only 0.0132 km. Fig. 5c shows the magnetic anomalies obtained from the application of Eq. (1) to the estimated interface in Fig. 5b. From Fig. 5a and c, the interface relief obtained from inversion produces a magnetic anomaly map very close in shape to the theoretical anomaly map. The difference between the actual and calculated magnetic anomalies is shown in Fig. 5e. In this case, the calculation of the

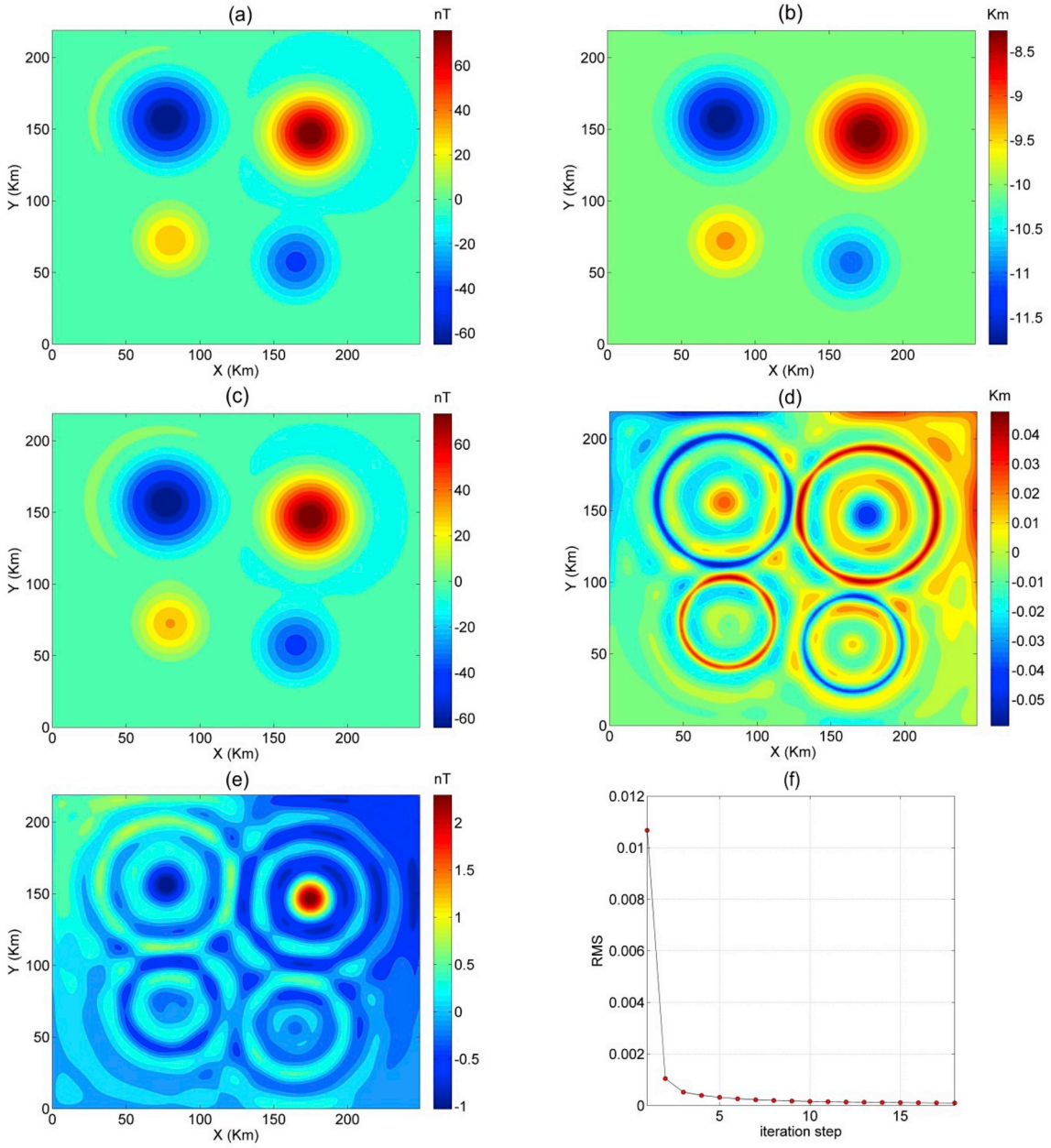

Fig. 4. The first synthetic example with an inclination of 90° and a declination of −3°. (a) theoretical magnetic anomalies (b) the inverted depth of the model, (c) magnetic anomalies obtained from the inverted interface, (d) the difference between the actual and inverted depth, (e) the difference between actual and calculated magnetic anomalies, (f) variation of RMS error against the iteration number.

depth to the basement from the magnetic anomalies on a 220× 250 grid, took only about 3.5 s.

The sensitivity of the MagB_inv program to random noise is analyzed by means of the third model. Here, we added random noise with amplitude equal to 10% of the anomaly amplitude to the data in Fig. 5a. Fig. 6a displays the noise-corrupted data. In this case, the roll-off frequency parameters of the low-pass filter have been chosen as SH = 0.065 and WH = 0.03. The inversion algorithm provides the depth interface shown in Fig. 6b. Although the data are noisy, the computed depth result compares reasonably with the corresponding depth model. The difference between the computed and the actual interface is shown in Fig. 6d. The RMS error between them is 0.0246 km. We note that, the noise effect has been reduced due to the low-pass filtering application during the iterative process. The corresponding modeled magnetic anomalies (Fig. 6c) closely match up with the model theoretical anomalies (Fig. 6a). The difference between the actual and calculated magnetic anomalies is shown in Fig. 6e. In this case, the inversion process performed twenty iterations where the RMS error between two successive approximations has reduced from 0.0117 km to 9.6132×10^{-5} km (Fig. 6f), and the computation time was only 3.8 s.

5. Real data application

An application to real data of the program is illustrated by inverting total intensity magnetic anomalies from northwest Germany (Hahn et al., 1976). The study area is located in the southeastern part of North Sea basin (Fig. 7).

Fig. 8 shows the total magnetic intensity map of the area (Hahn et al., 1976). It was digitized and interpolated into a regular grid with 30 × 54 points in north and east directions, respectively. These magnetic anomalies were previously used to determine the regional magnetic basement relief (Hahn et al., 1976; Pustisek, 1990). Pustisek (1990) used

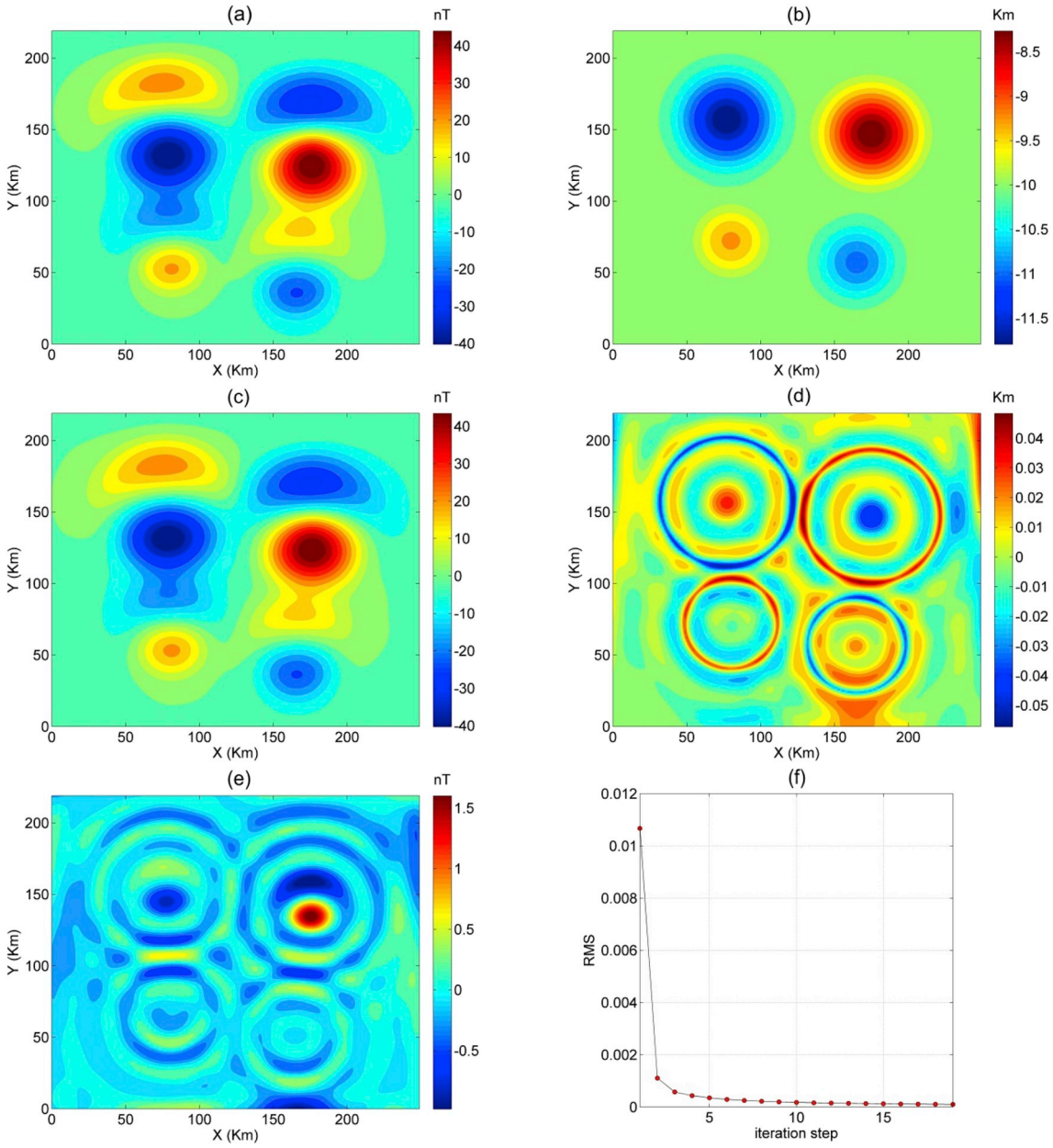

Fig. 5. The second synthetic example with an inclination of 40° and a declination of −3°. (a) theoretical magnetic anomalies (b) the inverted depth of the model, (c) magnetic anomalies obtained from the inverted interface, (d) the difference between the actual and inverted depth, (e) the difference between actual and calculated magnetic anomalies, (f) variation of RMS error against the iteration number.

inclination and declination of the magnetization of 68.2° and −3.1°, respectively and the magnetization direction is assumed to be parallel to the direction of the ambient field. Other input parameters used in the present inversion were: a mean depth for magnetic basement interface of 13 km (Pustisek, 1990) and a magnetization contrast of 2 A/m (Hahn et al., 1976). To obtain the convergence of the iterative procedure, the roll-off frequency parameters of low-pass filter have been chosen as SH = 0.06 and WH = 0.03.

Fig. 9 shows the inverted depth to the crystalline magnetic basement. The obtained result shows that the depth to magnetic basement ranges from 9.4 to 16 km. The regional basement structural features and trends reported previously by Pratsch (1980) are also marked on Fig. 9 for comparison. Hereby, it can be observed that all the regional basement structural features and trends are well reflected on the inverted basement structure. Fig. 10a shows the magnetic anomalies obtained from the application of Eq. (1) to the estimated depth configuration. Although the geometry of the recalculated magnetic anomaly is similar to the observed one, there is a small difference between them due to the use of the low pass filter which lead to loss of high frequency information. By setting the threshold value of the presumed accuracy to 10^{-3} km, the code performed thirty-one iterations with a RMS error between two successive approximations reducing from 0.119 km to 9.8942×10^{-4} km (Fig. 11).

The observed magnetic anomalies of the area also have been interpreted previously by Hahn et al. (1976) using the statistical spectral method, and by Pustisek (1990) using the Schmidt-Lichtenstein nonlinear approach. According to Pustisek (1990), the inverted interface obtained from the Schmidt-Lichtenstein nonlinear approach matches reasonably with the result reported by Hahn et al. (1976). For comparison, Fig. 10b displays the reported model by Hahn et al. (1976) that shows a basement relief in 9–16 km range depth. It is obvious that our results are in agreement with the depths reported by Hahn et al.

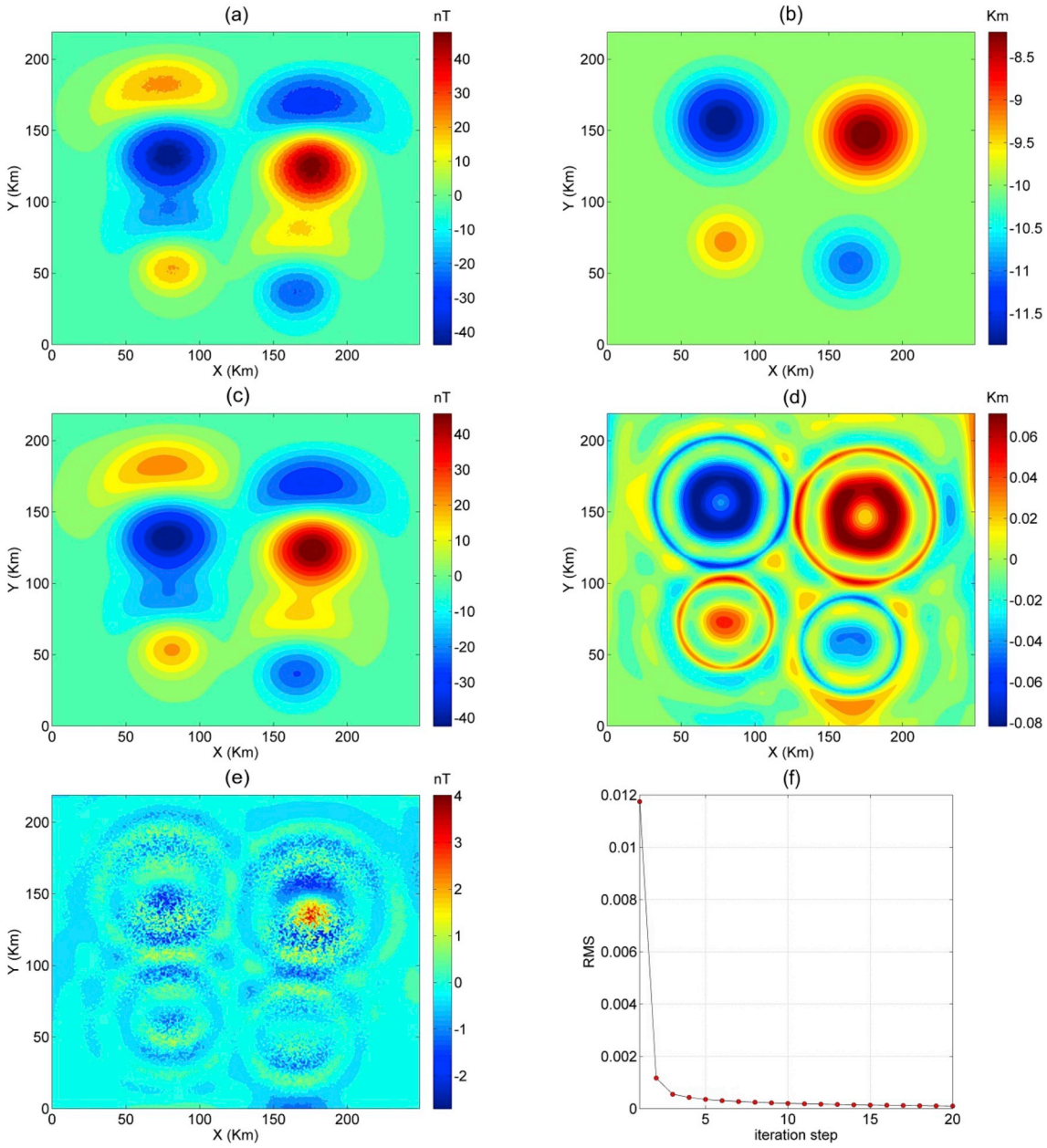

Fig. 6. The third synthetic example with an inclination of 40° and a declination of −3°. (a) theoretical magnetic anomalies with 10% noise (b) the inverted depth of the model, (c) magnetic anomalies obtained from the inverted interface, (d) the difference between the actual and inverted depth, (e) the difference between actual and calculated magnetic anomalies, (f) variation of RMS error against the iteration number.

(1976). In general, the basement structure obtained from the present code is comparable with the one reported by Hahn et al. (1976). However, unlike the solution obtained by Hahn et al. (1976), the inverted basement interface from our program has revealed the presence of a regional basement element, called the Bramsche high trend (H–V), which is also well reflected in the regional structural map of northwestern Germany by Pratsch (1979, 1980).

6. Conclusion

A GUI based Matlab code, MagB_inv program, is developed to map the relief of a crystalline magnetic basement from observed magnetic anomalies. The code is based on the rearrangement of a relation between the Fourier transform of magnetic anomaly and the Fourier transform of the function describing the surface between two magnetic layers. The present code can perform fast computation with high precision. Hence, it also proves to be an efficient tool in handling large data sets. The applicability and validity of the present code was tested on both synthetic and real magnetic data. In case of synthetic example, we analyze (1) magnetic anomalies caused by vertical magnetization model, (2) magnetic anomalies caused by non-vertical magnetization model, and (3) anomalies caused by non-vertical magnetization model in the presence of pseudorandom noise. The obtained results demonstrate the high performance of the developed code in determining the magnetic basement structure. Further, as a real data application, the inverted depth of the crystalline magnetic basement interface from the data of northwest Germany matches very well with those obtained from previous studies. Consequently, we conclude that the developed code has proven to be useful in determining the 3D structure of the crystalline magnetic basement from magnetic data sets. Thus it can be considered a favorable tool for both geophysical exploration and deep crustal geophysical research applications.

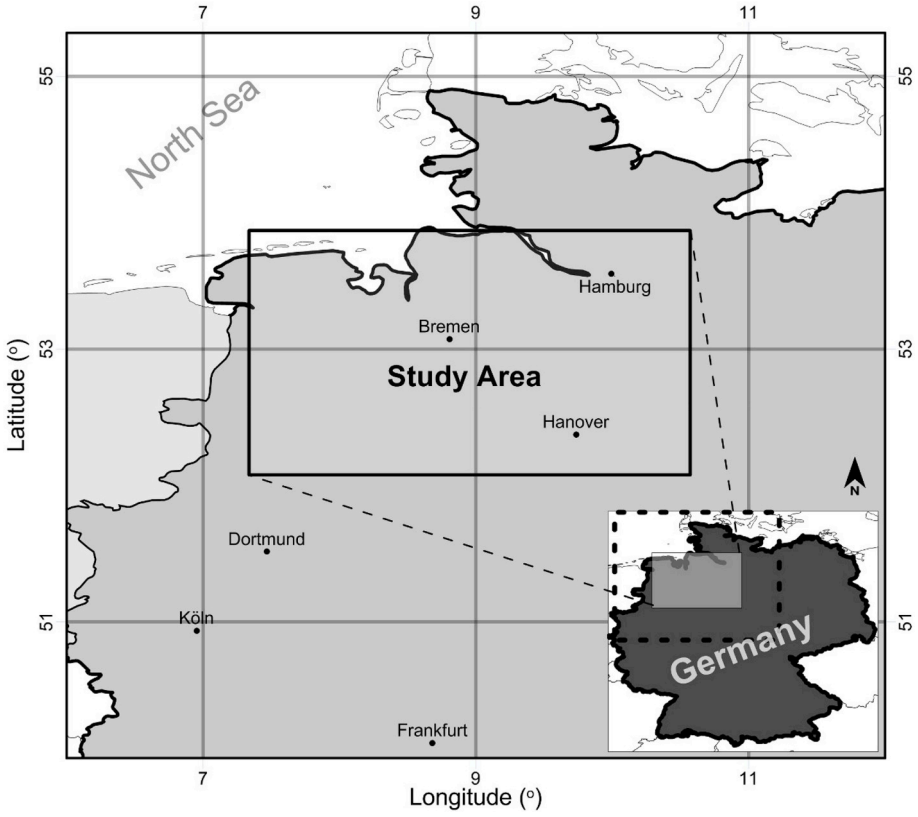

Fig. 7. The area of the real data application.

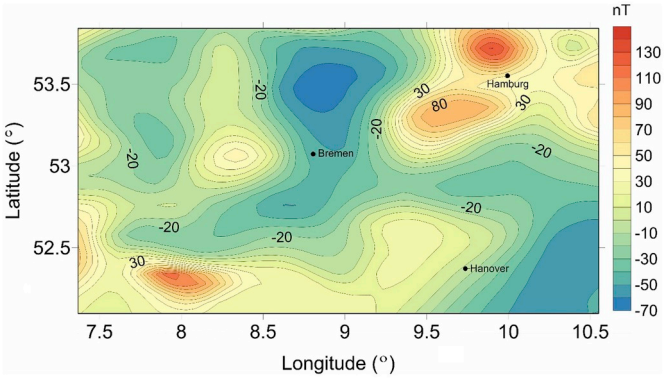

Fig. 8. Total field magnetic anomalies of the study area in NW Germany (after Hahn et al., 1976).

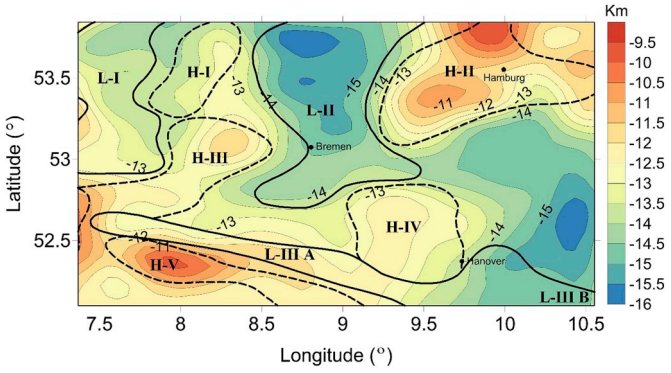

Fig. 9. Magnetic basement topography obtained in this study by inverting the magnetic field of the study area. The regional basement structural features and trends (after Pratsch, 1980) are also shown. *L-I:* Ems low trend, *L-II:* Bremen low trend, *L-III A:* lower Saxonian low trend, *L-III B:* Subhercynian low trend, *H–I:* north Oldenburg high trend, *H-II:* Hamburg High trend, *H-III:* Oldenburg High trend, *H-IV:* Walsrode High, *H–V:* Bramsche High trend.

Computer code availability

Name of code: MagB_inv.m

Developer:

- Luan Thanh Pham (contact address: VNU University of Science, Faculty of Physics, 334 Nguyen Trai, Thanh Xuan, Hanoi, Vietnam; e-mail: luanpt@hus.edu.vn).
- Erdinc Oksum (contact address: Süleyman Demirel University, Engineering Faculty, Department of Geophyisical Engineering, 32260 Isparta, Turkey; e-mail: eroksum@gmail.com)

Year first available: 2019
Hardware required: Windows PC
Software required: Matlab (version R2013b or higher)
Program language: Matlab
Graphical User Interface Gui: provided
Program size: 44 KB
How to access the source code:
The MagB_inv.m program is an open source code and can be obtained from the web site [https://github.com/PhamLT/MagB] or from the corresponding author for use in many geophysical and tectonic problems.

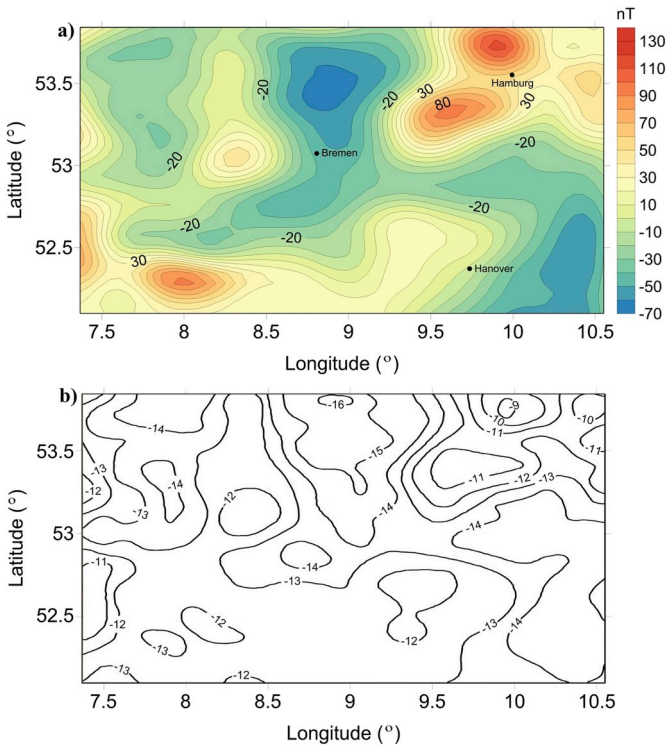

Fig. 10. (a) Magnetic field recalculated from the inverted basement topography, (b) Magnetic basement topography reported by Hahn et al. (1976).

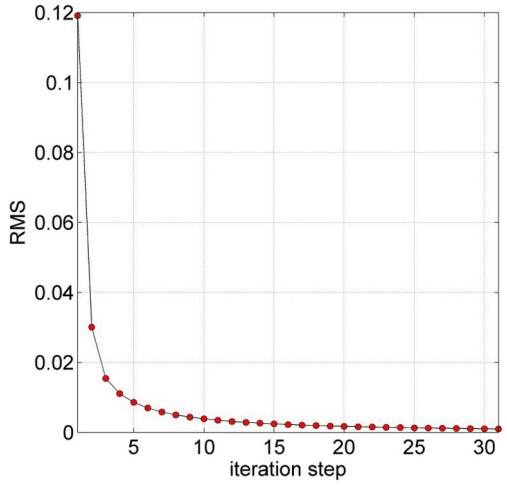

Fig. 11. Variation of RMS error against the iteration number for the real data application.

Author contributions

Luan Thanh Pham contributed to establish the basis of the algorithm and to the development of kernel codes.

Erdinc Oksum contributed to the creation of the main code of the program linked to the algorithm.

David Gómez-Ortiz contributed to the article writing and to its scientific development.

Thanh Duc Do contributed to provide feedback to improve the manuscript.

Declaration of competing interest

The authors declare that they have no known competing financial interests or personal relationships that could have appeared to influence the work reported in this paper.

Acknowledgements

The authors record with pleasure their sincere thanks to the editor Dario Grana and the two anonymous reviewers for their very constructive suggestions to improve the manuscript.

Appendix A. Supplementary data

Supplementary data to this article can be found online at https://doi.org/10.1016/j.cageo.2019.104347.

References

Abdullahi, M., Kumar, R., Singh, U.K., 2019. Magnetic basement depth from high-resolution aeromagnetic data of parts of lower and middle Benue Trough (Nigeria) using scaling spectral method. J. Afr. Earth Sci. 150, 337–345.

Al-Badani, M.A., Al-Wathaf, Y.M., 2017. Using the aeromagnetic data for mapping the basement depth and contact locations, at southern part of Tihamah region, western Yemen. Egypt. J. Pet. 27 (4) https://doi.org/10.1016/j.ejpe.2017.07.015.

Al-Garni, M.A., 2010. Magnetic survey for delineating subsurface structures and estimating magnetic sources depth, Wadi Fatima, KSA. J. King Saud Univ. Sci. 22 (2), 87–96.

Aydin, I., Oksum, E., 2010. Exponential approach to estimate the Curie-temperature depth. J. Geophys. Eng. 7, 113–125.

Aydın, I., Oksum, E., 2012. MATLAB code for estimating magnetic basement depth using prisms. Comput. Geosci. 46, 183–188.

Blakely, R.J., 1995. Potential Theory in Gravity and Magnetic Applications. Cambridge University Press, Cambridge, pp. 278–294.

Blakely, R.J., 1988. Curie temperature isotherm analysis and tectonic implications of aeromagnetic data from Nevada. J. Geophys. Res. 93, 11817–11832.

Brimich, L., Khalil, A., Kordik, P., Mekkawi, M., El-Bohoty, M., Refai, M.K., Kader, A.K. A., 2011. Active subsurface structures at Fayoum-Cairo district, Northern Western Desert, Egypt, as deduced from magnetic data. Contrib. Geophys. Geodes. 41 (4), 329–351.

Caratori Tontini, F., Cocchi, L., Carmisciano, C., 2008. Potential-field inversion for a layer with uneven thickness: the Tyrrhenian Sea density model. Phys. Earth Planet. Inter. 166, 105–111.

Caratori Tontini, F., 2012. Rapid interactive modeling of 3D magnetic anomalies. Comput. Geosci. 48, 308–315.

Chen, G., Cheng, Q., Zhang, H., 2016. Matched filtering method for separating magnetic anomaly using fractal model. Comput. Geosci. 90, 179–188.

Connard, G., Couch, R., Gemperle, M., 1983. Analysis of aeromagnetic measurements from the Cascade Range in central Oregon. Geophysics 48, 376–390.

Curto, J.B., Diniz, T., Vidotti, R.M., Blakely, R.J., Fuck, R.A., 2015. Optimizing depth estimates from magnetic anomalies using spatial analysis tools. Comput. Geosci. 84, 1–9.

Gomez-Ortiz, D., Agarwal, B.N.P., 2005. 3DINVER.M: a MATLAB program to invert gravity anomaly over a 3-D horizontal density interface by Parker-Oldenburg's algorithm. Comput. Geosci. 31, 513–520.

Hahn, A., Kind, E.G., Mishra, D.C., 1976. Depth estimation of magnetic sources by means of Fourier amplitude SPECTRA*. Geophys. Prospect. 24 (2), 287–306.

Hansen, R.O., Simmonds, M., 1993. Multiple-source werner deconvolution. Geophysics 58, 1792–1800.

Hansen, R.O., 2005. 3D multiple-source Werner deconvolution for magnetic data. Geophysics 70 (5), L45–L51.

Hartman, R.R., Teskey, D.J., Friedberg, J.L., 1971. A system for rapid digital aeromagnetic interpretation. Geophysics 36, 891–918.

Jiang, F., Wu, J., Wang, J., 2008. Joint inversion of gravity and magnetic data for a two-layer model. Appl. Geophys. 5 (4), 331–339.

Kilty, K.T., 1983. Werner deconvolution of profile potential field data. Geophysics 48, 234–237.

Martelet, G., Perrin, J., Truffert, C., Deparis, J., 2013. Fast mapping of magnetic basement depth, structure and nature using aeromagnetic and gravity data: combined methods and their application in the Paris Basin. Geophys. Prospect. 61 (4), 857–873.

Maus, S., 1999. Variogram analysis of magnetic and gravity data. Geophysics 64, 776–784.

Maus, S., Sengpiel, K.P., Rottger, B., Tordiffe, E.A.W., 1999. Variogram analysis of helicopter magnetic data to identify paleochannels of the Omaruru River, Namibia. Geophysics 64, 785–794.

Mendel, V., Munschy, M., Sauter, D., 2005. MODMAG, a MATLAB program to model marine magnetic anomalies. Comput. Geosci. 31 (5), 589–597.

Nabighian, M.N., Hansen, R.O., 2001. Unification of Euler and Werner deconvolution in three dimensions via the generalized Hilbert transform. Geophysics 66, 1805–1810.

Oldenburg, D.W., 1974. The inversion and interpretation of gravity anomalies. Geophysics 39 (4), 526–536.
Parker, R.L., 1972. The rapid calculation of potential anomalies. Geophys. J. R. Astron. Soc. 31, 447–455.
Pham, L.T., Do, T.D., Oksum, E., Le, S.T., 2019. Estimation of Curie point depths in the Southern Vietnam continental shelf using magnetic data. Vietnam J. Earth Sci. 41 (3), 116–228.
Pham, L.T., Oksum, E., Do, T.D., 2018. GCH_gravinv: a MATLAB-based program for inverting gravity anomalies over sedimentary basins. Comput. Geosci. 120, 40–47.
Pilkington, M., Crossley, D.J., 1986. Determination of crustal interface topography from potential fields. Geophysics 51, 1277–1284.
Pilkington, M., 2006. Joint inversion of gravity and magnetic data for two-layer models. Geophysics 71, L35–L42.
Pratsch, J.C., 1979. Regional structural elements in Northwest Germany. J. Pet. Geol. 2, 159–180.
Pratsch, J.C., 1980. Basement deformation and basement structure in the Northwest German basin. Int. J. Earth Sci. 69 (3), 609–621.
Pustisek, A.M., 1990. Noniterative three-dimensional inversion of magnetic data. Geophysics 55 (6), 782–785.
Reid, A.B., Allsop, J.M., Granser, H., Millett, A.J., Somerton, I.W., 1990. Magnetic interpretation in three dimensions using Euler deconvolution. Geophysics 55, 80–91.
Salem, A., Green, C., Cheyney, S., Fairhead, J.D., Aboud, E., Campbell, S., 2014. Mapping the depth to magnetic basement using inversion of pseudogravity: application to the Bishop model and the Stord Basin, northern North Sea. Interpretation 2 (2), T69–T78.
Schettino, A., 2012. Magan: a new approach to the analysis and interpretation of marine magnetic anomalies. Comput. Geosci. 39, 135–144.
Shin, Y.H., Choi, K.S., Xu, H., 2006. Three-dimensional forward and inverse models for gravity fields based on the Fast Fourier Transform. Comput. Geosci. 32 (6), 727–738.
Spector, A., Grant, F.S., 1970. Statistical models for interpreting aeromagnetic data. Geophysics 35, 293–302.
Thompson, D.T., 1982. EULDPH: a new technique for making computer-assisted depth estimates from magnetic data. Geophysics 47, 31–37.
Vo, S.T., 2003. Interpretation of the aeromagnetic map ΔTa of the Tuan Giao region using Euler deconvolution. Vietnam J. Earth Sci. 25 (2), 112–116.
Werner, S., 1953. Interpretation of magnetic anomalies at sheet-like bodies: Sveriges Geologiska under. Ser. C.C. Arsbok 43 (06).
Xia, J., Sprowl, D.R., Adkins-Heljeson, D., 1991. A Fast and Accurate Approach: Correction of Topographic Distortions in Potential-field Data. SEG Technical Program Expanded Abstracts. https://doi.org/10.1190/1.1889187, 1991.
Zhang, C., Huang, D.N., Zhang, K., Pu, Y.T., Yu, P., 2016. Magnetic interface forward and inversion method based on Padé approximation. Appl. Geophys. 13 (4), 712–720.